J. Fluid Mech. (2004), *vol.* 518, *pp.* 157–185.
DOI: 10.1017/S0022112004000928 Printed in the United Kingdom

Coalescence and bouncing of small aerosol droplets

By GLORIA A. BACH, DONALD L. KOCH AND ARVIND GOPINATH

School of Chemical Engineering, Cornell University, Ithaca, NY 14853, USA

(Received 13 June 2002 and in revised form 14 June 2004)

The trajectories of 20 and 40 μm radius water droplets colliding with a gas–water interface are observed to determine the conditions under which drops will bounce or coalesce on impact and the apparent coefficient of restitution of the drops that bounce. The experiments were performed in a pressure chamber so that the pressure and composition of the gas could be varied to explore the effects of the viscosity and mean-free path of the gas. The impact velocity is varied by producing drops with a velocity larger than their terminal velocity using a piezoelectric drop generator and adjusting the distance between the generator and the liquid interface. The geometry of the collisions is axisymmetric and the Weber number, $We = \rho_l U^2 a/\sigma$, is $O(1)$ or smaller, so as to facilitate comparison with a theory for weakly deformable gas–liquid interfaces. Here, ρ_l is the liquid density, U the impact velocity, a the drop radius and σ the surface tension. After a low-Weber-number drop coalesces, a smaller, daughter drop is emitted from the interface with a velocity higher than the incident velocity of the mother drop. The daughter drop radius is about $0.55a$ and the daughter velocity is $0.38(\sigma/(\rho_l a))^{1/2}$ for $We < 0.01$.

The experimental results are compared with a theory in which the small deformations of the drop and surface are expanded in Legendre polynomials and Fourier modes, respectively, the non-continuum lubrication stresses are computed in the thin gas film between the drop and interface, and the liquid flow is approximated as an inviscid potential flow. The coefficient of restitution decreases with increasing Weber number and becomes insensitive to the viscosity of the gas at Weber numbers larger than about 1. At smaller Weber numbers, drops in a less viscous gas lose less energy during the collision. Drops are observed to undergo a transition from coalescence to bouncing as the drop velocity (Weber number) is increased. However, the marginal condition for drop bouncing is much more sensitive to gas mean-free path (Knudsen number) and gas viscosity (Ohnesorge number) than to Weber number. The Knudsen and Ohnesorge numbers are defined as $Kn = \lambda/a$ and $Oh = \mu_g/(\rho_l a \sigma)^{1/2}$ where λ is the mean-free path and μ_g is the gas viscosity. Theory and experiment show similar trends of increasing critical Weber number with decreasing Ohnesorge number and increasing Knudsen number. Theoretical results are also derived for the coalescence–bounce transition and coefficient of restitution for head-on collisions of equal sized drops.

1. Introduction

When a drop collides with a fluid interface or with another drop, the collision may result in bouncing, coalescence, or coalescence followed by re-emission of one

or more drops. The outcome of drop–drop collisions plays an important role in the development of the drop size distribution in dense sprays. The collision of a drop with a fluid interface retains much of the physics of a drop-drop collision but is more easily observed experimentally. In addition drop–interface collisions may influence the concentration of drops and the thickness of a liquid film in situations, such as gas–vapour heat exchangers, where a spray of droplets coexists with a continuous liquid phase (Lee & Hanratty 1988). Droplet bouncing may also be a phenomenon that one would like to avoid in designing drop-on-demand technologies where small quantities of fluids are to be delivered as aerosol droplets to specific positions on a surface. Previous experimental studies of drop–drop and drop–interface collisions in a gas have involved drops larger than about 100 μm in diameter. We will examine smaller drops (40 and 80 μm diameter) in order to explore the different physics that arises with small drop size and to facilitate comparison with a theory based on small-amplitude deformation of the surface of the drop and the gas–liquid interface. For simplicity of analysis, axisymmetric collisions are studied. Before a drop can coalesce with a fluid layer or another drop, the thin gas film separating the two gas–liquid interfaces must break down. This suggests the possibility that non-continuum gas flow may play a critical role in the coalescence–bounce transition. To investigate this possibility, our experiment allows for variation of the pressure and composition of the gas and our theory incorporates the rarefied gas flow occurring in the lubrication gas film.

When aerosol drops bounce from a liquid surface, they typically have sufficient inertia to travel far away from the surface before gravity pulls them back to undergo a second collision. Furthermore, the influence of gravity during the actual collision is small (Gopinath & Koch 2001*a*, *b*). This may be contrasted with the case of liquid drops suspended in a liquid where the energy of the drop is dissipated quickly by the viscosity of the suspending fluid and gravity plays an important role during the collision. Since drop–interface and drop–drop collisions are quite similar in aerosol systems, we will consider both types of collision in our theoretical study. Our experimental study will focus on drop–interface collisions because they are more easily produced and observed than drop–drop collisions.

The seminal experimental study of coalescence of water drops at a gas–water interface was published by Schotland (1960). Schotland observed the oblique collision of a stream of drops with a gas–liquid interface and varied the pressure and composition of the gas. For drops of diameter 200–800 μm, he found that the outcome of the collision depended on the Weber number, $We = \rho_l U_n^2 a/\sigma$, based on the component of the velocity normal to the surface, U_n, and on the ratio of densities of the gas and liquid phases, ρ_g/ρ_l. Here, ρ_l and ρ_g are the densities of the liquid and gas phases, a is the drop radius, and σ is the interfacial tension. The Weber numbers considered by Schotland were quite large and his observations are consistent with the assumption that fluid and gas inertia were predominant mechanisms controlling the outcome of the collision. Drops with sufficiently high inertia coalesced whereas lower Weber number drops bounced.

Jayaratne & Mason (1964) studied the oblique collision of a stream of water drops with an air–water interface for drop diameters of 120 to 400 μm at standard atmospheric conditions. In contrast to Schotland's experiments, Jayaratne & Mason observed a transition from coalescence at low Weber numbers to bouncing at moderate Weber numbers. The transition Weber numbers were typically $O(1)$ and depended in a non-monotonic fashion on the impact angle. Jayaratne & Mason also observed the coefficient of restitution for drops colliding with nearly normal impact velocity

to be about 0.2 for the range of Weber numbers from 0.8 to 16 considered in their study.

Later studies (Brazier-Smith, Jennings & Latham 1972) of drop–drop collisions showed a transition from coalescence to bouncing followed by a second transition from bouncing to coalescence with increasing Weber number at a given impact angle. Pairs of water drops at standard atmospheric conditions did not exhibit the first (coalescence-to-bouncing) transition if the impact velocity was nearly parallel to the line of centres. However, later studies (Qian & Law 1997) showed that the first transition occurs for nearly head-on collisions of hydrocarbon drops at standard atmospheric conditions and of water drops at elevated pressures. Qian & Law also noted that mass density is not the only property of the gas that affects the outcome of collisions. In particular, they found that drops bounced much more readily in helium at a pressure of 7.5 atm than in nitrogen at 1 atm despite the fact that the mass densities were identical. They noted that the helium has about 11% higher viscosity and that this might enhance the drop deformation and bouncing. However, we believe that a much more significant factor is the mean free path, which is 2.5 times smaller in the helium than in the nitrogen. Thus, non-continuum effects would reduce the lubrication pressure before the bounce could occur in nitrogen, but not in the higher-pressure helium.

The focus of this study will be to understand the initial transition from coalescence to bouncing that occurs at relatively modest Weber numbers. For simplicity of the experimental situation, we consider drop–interface collisions, while axisymmetric collisions are studied to simplify the theoretical calculations. In order for a drop to bounce, its kinetic energy must be converted to energy associated with the larger surface area of a deformed drop and interface and then restored to the kinetic energy associated with the motion of the drop away from the surface. At asymptotically small Weber numbers, this process can occur with interfacial deformations that are small compared with the radius of the drop. Exploiting this observation, Gopinath & Koch (2001*a*) developed an asymptotic theory for the dynamics of drop–drop collisions. In some of their calculations, the drops were considered to be separated by a repulsive boundary that prevented coalescence without any viscous dissipation of energy. In other calculations, viscous lubrication flow of the gas in the gap between the particles was considered. In this paper, we will account for the non-continuum gas flow in the lubrication film in order to predict the transition from coalescence to bouncing with decreasing gas mean-free path. The collision of a drop with a liquid surface was studied by Gopinath & Koch (2001*b*) using the simple model of a repulsive force preventing coalescence to determine the time scale of the bounce and the area of the near-contact region between the drop and interface. The present study provides the first analysis of the continuum or non-continuum gas flow in the lubrication film between a drop and a liquid surface. Thus, we will present results for the gas pressure and interfacial deformation profiles and obtain the coefficient of restitution for the bounce and the conditions leading to a coalescence–bounce transition.

The experimental method and the experimental observations of the coalescence–bounce transition and the coefficient of restitution will be discussed in § 2. In § 3, we discuss the theoretical method for describing drop–interface collisions incorporating non-continuum gas flow in the lubrication gap. The predictions of the theory for coalescence–bounce transition and coefficient of restitution are compared with the experimental observations in §§ 4 and 5, respectively. In § 6, we present experimental observations of the formation of smaller drops following a drop–interface coalescence event.

2. Experimental study of drop–interface collisions

We observed the collision of water drops of approximately 20 and 40 μm radius with a gas–water interface in a controlled atmosphere. The drops were formed from deionized water using a commercial Microdrop generator system developed by Gesselschaft fur Mikrodosiersysteme. This device produces drops of precisely controlled size from a glass capillary. The ejection process is forced by a piezo-ceramic that surrounds the capillary and compresses it with a controlled amplitude and duration so that a single drop can be formed with no satellite drops. The drop radius is varied primarily by changing the diameter of the capillary. There is also a slight dependence of the drop radius on the viscosity and pressure of the gas. The early work of Schotland and Jayaratne & Mason used streams of drops which facilitated observation with strobe photography. However, a stream of drops precludes observation of axisymmetric collisions because the bouncing drops would collide with the incoming drops. The Microdrop generator can form drops one at a time so that there is no interference between successive drops.

The drop generator is enclosed in an aluminium pressure vessel with quartz viewing windows, so that the gas composition and pressure can be varied. Nitrogen ($\mu_g = 1.66 \times 10^{-4}\,\mathrm{g\,cm^{-1}\,s^{-1}}$) and methane ($\mu_g = 1.02 \times 10^{-4}\,\mathrm{g\,cm^{-1}\,s^{-1}}$) were used as the ambient gases to explore the effects of gas viscosity. The apparatus was designed to allow a large range of pressures to be explored. However, for the drop sizes studied, coalescence–bounce transitions were only observed in a narrow range of pressures (2.8–3.5 atm for the larger drops and 4.5–6 atm for the smaller).

Drops are ejected from the capillary with a velocity of about $200\,\mathrm{cm\,s^{-1}}$. The impact velocity can be varied between this value and the terminal velocity of the drop by adjusting the vertical separation between the tip of the capillary and the gas–liquid surface using a translation mount. A 40 μm diameter drop reaches its terminal velocity of about $6\,\mathrm{cm\,s^{-1}}$ after falling approximately 3 cm in nitrogen at standard atmospheric conditions.

The trajectories of the drops as they collided with and bounced from the gas–liquid interface were observed using a high-speed video camera with 2000 frames/s attached to a long-range microscope. Despite the magnification, the drop radius was only a few pixels and so it could not be determined accurately from the video image. Instead, the drop radius was deduced from the apparent drag coefficient obtained by fitting the drop trajectory. The frame rate of our camera was not sufficient to observe the details of the drop bounce. This is not surprising because the time for which the drop is in near-contact with the surface is predicted to be about $t_b = 5(\rho_l a^3/\sigma)^{1/2} = 0.15\,\mathrm{ms}$ for the 40 μm radius drops (Gopinath & Koch 2001*b*). Thus, the information obtained from the experiment is a series of particle positions as a function of time before and after collision. A typical trajectory in which a drop bounces from the interface is plotted in figure 1. The trajectories were fitted to the results of a solution of the drop's equation of motion including inertia, gravity and nonlinear drag. The Reynolds number, $Re_g = \rho_g U a/\mu_g$, is typically of order one. An empirical nonlinear drag force suggested by Clift, Grace & Weber (1978) was adopted. The parameters obtained by fitting the trajectory were the incident velocity, rebound velocity and drop radius. Although multiple parameters were used to obtain a good fit, the interaction among these parameters was not a major source of error. The drag force (and therefore the drop radius) primarily affects the trajectory during the time after the bounce where the drop is approaching its terminal velocity, whereas the impact and rebound velocities control the trajectory close to the time of impact. The uncertainty in the drop radius and the coefficient of restitution determined by repeating measurements

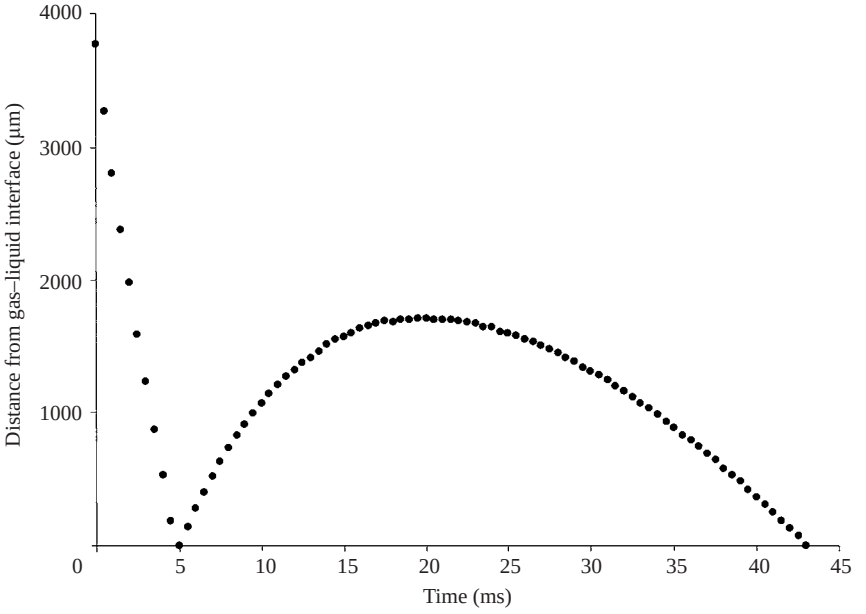

FIGURE 1. A typical trajectory in which a drop bounces from the interface.

for the same experimental conditions were about 5% and 3% of the mean values.

The dimensional parameters that might be expected to influence the outcome of the drop–interface collision are the interfacial tension σ, the density ρ_l of the liquid phase, the viscosity μ_g of the gas phase, the drop radius a, and the impact velocity U. The drop collision is not expected to be affected by the liquid viscosity μ_l or the gas density ρ_g for reasons that will be discussed in § 3. For coalescence to occur, the gas film between the drop and the pool of liquid must rupture. Because the dynamic viscosity of the liquid is larger than that of the gas, the gas velocity in the film must nearly vanish at the gas–liquid interfaces. As a result, the continuum lubrication force in the film is quite large and this force must be overcome by the breakdown of the continuum flow in the gas before coalescence can occur. This leads to an additional dimensional parameter, the mean free path of the gas λ.

A convenient choice of dimensionless parameters is then the Knudsen number $Kn = \lambda/a$, the Ohnesorge number $Oh = \mu_g/(\rho_l a\sigma)^{1/2}$ based on the gas viscosity and the liquid density, and the Weber number $We = \rho_l U^2 a/\sigma$. The Ohnesorge and Knudsen numbers are fixed by the choice of drop size and the gas–liquid system. Thus, only the Weber number changes when we do a series of experiments varying drop velocity.

The results of our experiments are presented in figure 2 and table 1. The figure shows the coefficient of restitution e for drop–interface collisions that lead to a bounce as a function of the Weber number for two drop radii (approximately 20 and 40 μm) and for nitrogen and methane as the suspending gases. We did not observe any effect of gas pressure on the coefficient of restitution and the figure contains results for all the pressures considered in our study. The lack of dependence of the coefficient of restitution on pressure is to be expected. The gas viscosity is independent of pressure and the pressure affects only the mean free path of the gas. The mean free path modifies the viscous pressure drop in the gas film at very small separations and leads to a breakdown of the gas film. However, when drops bounce at Weber numbers

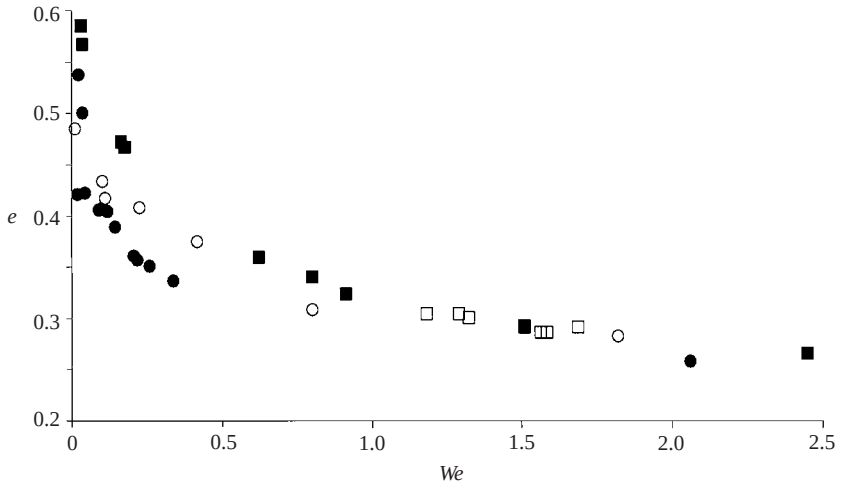

FIGURE 2. Experimental results for the coefficient of restitution e for drop–interface collisions as a function of the Weber number We. The open symbols are for the larger drops and the closed symbols for the smaller drops. The circles are experiments with nitrogen and the squares with methane. Each point on the plot represents an average of three drops generated under the same conditions.

Ambient gas	Average drop radius (μ)	χ	Ca	We	Kn	Oh	$\delta_{nc\_critical}$, experiment
N_2	19	305	7.36×10^{-5}	0.022	5.48×10^{-4}	4.91×10^{-4}	15.64
N_2	37	306	3.86×10^{-5}	0.012	5.46×10^{-4}	3.55×10^{-4}	11.38
CH_4	17	586	5.83×10^{-5}	0.034	5.55×10^{-4}	3.16×10^{-4}	13.77
CH_4	33	4825	2.46×10^{-4}	1.185	5.70×10^{-4}	2.26×10^{-4}	27.51
N_2	22	417	8.70×10^{-5}	0.036	6.96×10^{-4}	4.57×10^{-4}	13.40
N_2	41	996	1.12×10^{-4}	0.112	6.15×10^{-4}	3.36×10^{-4}	17.21
CH_4	18	2923	2.75×10^{-4}	0.804	6.97×10^{-4}	3.07×10^{-4}	23.79
CH_4	32	4946	2.61×10^{-4}	1.291	7.43×10^{-4}	2.30×10^{-4}	21.74

TABLE 1. Summary of experimental results for bounce–coalescence transitions.

significantly above the critical Weber number for the coalescence–bounce transition, the film thickness is expected to remain much larger than the mean free path and no effect of the gas pressure is anticipated. As the Weber number increases, the coefficient of restitution decreases. This may be attributed to the larger amplitude of interfacial deformation that occurs at larger Weber numbers. The larger deformation allows a greater portion of the drop's kinetic energy to be transformed into waves on the liquid surface and oscillations of the drop shape. At high Weber number, the coefficient of restitution is independent of the gas viscosity as may be expected if the energy loss to surface waves dominates over viscous dissipation. The results for Weber numbers greater than one approach a coefficient of restitution of approximately 0.3, which is near the value of about 0.2 obtained by extrapolating Jayaratne & Mason's (1964) observations for $We = 0.8 - 16$ to normal incidence. At smaller Weber numbers, the coefficients of restitution for drops in the less viscous methane gas exceed those in nitrogen. Similarly, the larger drops in nitrogen have a higher coefficient of restitution than the smaller drops in nitrogen. An increase in the radius of the drop decreases

the Ohnesorge number, which may be viewed as a non-dimensional viscosity, and so an increase in the coefficient of restitution is to be expected. We may note that the coefficient of restitution for all the conditions studied is low. The fraction of the kinetic energy retained after the collision, i.e. e^2, is always less than 0.4.

When a drop approaches the interface with a small velocity, it produces small fluid dynamic stresses and little deformation of the interface and coalesces on impact. As the drop velocity (or Weber number) is increased, the extent of the drop and interface deformation increases. This leads to the possibility that the kinetic energy associated with the drop's translational motion will be stored as interfacial energy and then converted back to kinetic energy of drop motion in the opposite direction. The lowest Weber numbers for which drops were observed to bounce are given in table 1 for two values of the drop radius (approximately 20 and 40 μm) in gases (methane and nitrogen) with two viscosities. The gas pressure was in the range 2.8–6 atm and was adjusted to give two values of the Knudsen number (approximately 5.5×10^{-4} and 6.9×10^{-4}). The results in table 1 clearly indicate that gas pressure has a strong influence on the coalescence–bounce transition. As the pressure is decreased so that the mean free path and Knudsen number increase, continuum lubrication interactions break down at a larger gap thickness. This extends the range of Weber numbers for which coalescence occurs. Originally, we planned to perform experiments over a much wider range of gas pressures. However, we found that outside a narrow range of pressures, either all drops coalesce or all drops bounce for the range of impact velocities accessible with our apparatus. The experiments conducted in methane, the gas with the lower viscosity (yielding a smaller Ohnesorge number), exhibited a higher critical Weber number. In the less viscous gas, the gas film must thin to a smaller gap thickness before the drop and interface deform sufficiently to produce a bounce. Thus, the liquid–gas interfaces come closer together and have more opportunity to coalesce. Increasing the drop radius also decreases the Ohnesorge number, which may be thought of as a non-dimensional gas viscosity. This helps us understand why an increase in drop radius also leads to a higher critical Weber number. Note that when we increased the drop radius we also adjusted the pressure so that the Knudsen number remained unchanged.

3. Theoretical description of collisions

Most previous investigations of drop–drop and drop–interface collisions in the parameter regime characteristic of aerosol drops have not incorporated a detailed study of the role of the gas film in the collision. For example, Foote (1975) used an artificial repulsive barrier to prevent drop–drop contact and computed the radial extent and temporal duration of the contact event. He then used this information to solve a separate film drainage problem and applied a criterion that when the film reached a specified thickness rupture must occur. Similarly, Gopinath & Koch (2001*b*) studied the inviscid dynamics of a drop–interface collision using an artificial repulsive barrier and found the time of the bounce and maximum extent of the contact region as a function of the Weber number. Nobari, Jan & Tryggvason (1996) used a finite-difference method to simulate the collision of two drops in a gas at high Weber numbers ($We = 10$–110). They determined the time scale of collision, the radial extent of the contact region and the coefficient of restitution, but did not resolve the flow in the gas film down to length scales at which non-continuum or non-hydrodynamic effects might have led to coalescence.

To predict the transition from coalescence to bouncing and the coefficient of restitution for aerosol droplet collisions, we require a coupled solution of the non-continuum gas flow and interfacial deformation in the lubrication gap and the liquid flow and interfacial deformation outside the gap region. Gopinath & Koch (2001*a*) developed such a coupled solution for the head-on collision of two aerosol droplets in a continuum gas and that study will form the basis for the method employed here. The method is based on matched asymptotic expansions for the gas velocity and interfacial deformation in a lubrication film and an inviscid analysis of liquid flow in the drops or drop and fluid half-space. A characteristic thickness of the gas film during the bounce process is the gap thickness $aCa^{1/2}$ at which the lubrication pressure becomes comparable with the Laplace pressure σ/a so that significant drop deformation occurs. Here, $Ca = \mu_g U/\sigma$ is the capillary number. The lubrication analysis is applicable as long as this gap thickness is much smaller than a. We will impose a no-slip boundary condition on the gas velocity at the gas–liquid interfaces. This approximation is valid if $(\mu_g/\mu_l)^2 \ll Ca^{1/2} \ll 1$. In our experiments, $(\mu_g/\mu_l)^2 = 1\times10^{-4} - 2.8\times10^{-4}$ and $Ca^{1/2} = 6\times10^{-3} - 2\times10^{-2}$. The inertia in the gas film can be neglected as long as $Re_g Ca^{1/2} \ll 1$. A typical value of $Re_g Ca^{1/2}$ in our experiments is 0.01.

The larger length scale a of the flow of the liquid within the deforming drop and the liquid half-space and the smaller kinematic viscosity of the liquid make viscous effects in the liquid much less important than in the gas phase. A criterion for an inviscid analysis of the liquid flow is that the characteristic bounce time, $t_b = (\rho_l a^3/\sigma)^{1/2}$ be much smaller than the time $a^2\rho_l/\mu_l$ for viscous diffusion through the drop (Gopinath & Koch 2001*a*). For our experimental conditions, $t_b = 0.15$ ms and $a^2\rho_l/\mu_l = 1.6$ ms. The analysis assumes that the characteristic amplitude of drop and interface deformation, $aWe^{1/2}$ and the radial extent of the lubrication film $aWe^{1/4}$ are much smaller than the drop radius, although the drop–interface collisions in our experimental study occur at lower Weber numbers than previous experiments, $We^{1/4} = 0.3$–1.2. Thus, the assumption that there is a wide separation between the radial extents of the film and outer region is likely to lead to the most significant errors in applying the theory.

In applying the theory of Gopinath & Koch (2001*a*) to determine the coalescence–bounce transition, we must incorporate an analysis of the non-continuum gas flow in the lubrication region. In addition, the collision geometry and the conditions for matching the inner and outer solutions are different in the drop–interface collision that is our primary focus here and the drop–drop collisions considered by Gopinath & Koch (2001*a*). Thus, we will explain these two features in detail.

We consider an initially spherical aerosol drop approaching an initially planar gas–liquid interface with initial velocity $W^*(t^*=0) = -U\boldsymbol{k}$, where $\boldsymbol{k}$ is the unit normal pointing out of the liquid half-space. In this section, a superscript asterisk will denote dimensional variables, and scaled variables will have no asterisk. We denote the downward deformation of the interface from its initial plane as $D_1^*(r^*, t^*)$ and the upward deformation of the drop from its initial spherical shape as $D_2^*(r^*, t^*)$ where r^* is the radial distance from the axis of symmetry. We define a gap thickness $h^*(t^*)$ that would occur in the absence of deformation, so that $\mathrm{d}h^*/\mathrm{d}t^* = W^*$. The positions of the interface and the drop relative to the initial plane of the undeformed interface are $H_1^* = -D_1^*$ and $H_2^* = h^* + r^{*2}/(2a) + D_2^*$, respectively, and the gap between the two liquid–gas interfaces is $H^* = H_2^* - H_1^* = h^* + r^{*2}/(2a) + D_1^* + D_2^*$.

Interfacial deformation becomes important when the lubrication gas pressure is comparable to the Laplace pressure σ/a. This occurs at a gap thickness of $aCa^{1/2}$. Thus, we scale the pressure with σ/a, the gap thickness with $aCa^{1/2}$ and the radial

coordinate with $aCa^{1/4}$. Deformations are scaled with $aWe^{1/2}$, velocities with U, and times with the bounce time $aWe^{1/2}/U$. The scaled gap thickness is thereby

$$H = h + \tfrac{1}{2}r^2 + St^{1/2}(D_1 + D_2), \tag{1}$$

where $St = We/Ca = \rho_l Ua/\mu_g$ is the Stokes number which represents the relative importance of drop inertia and gas viscosity. Typically, $St^{1/2} = 17$–70 in our experimental study. The boundary conditions on the fluid velocity $\boldsymbol{u}$ are

$$u_r = 0 \quad \text{at} \quad z = H_1, \quad z = H_2, \tag{2}$$

$$u_z = -\frac{\partial D_1}{\partial t} \quad \text{at} \quad z = H_1, \tag{3}$$

and

$$u_z = W + \frac{\partial D_2}{\partial t} \quad \text{at} \quad z = H_2, \tag{4}$$

where z is the coordinate normal to the initial plane of the interface scaled with $aCa^{1/2}$.

Assuming that the primary force acting on the drop during the bounce is the lubrication pressure, the equation of motion for the drop yields

$$\frac{\mathrm{d}W}{\mathrm{d}t} = \frac{3}{2St^{1/2}} \int_0^\infty (p - p_\infty) r \, \mathrm{d}r, \tag{5}$$

where p_∞ is the ambient pressure.

The importance of non-continuum effects in the lubrication gas flow can be characterized by a ratio of the characteristic gap at which deformation occurs to the mean free path of the gas, i.e. $\delta_{nc} = aCa^{1/2}/\lambda$. When $\delta_{nc} = O(1)$, the flow of the gas in the gap is governed by the Boltzmann equation

$$\frac{\partial(n^* f^*)}{\partial t^*} + c_r^* \frac{\partial(n^* f^*)}{\partial r^*} + c_z^* \frac{\partial(n^* f^*)}{\partial z^*} = J(n^* f^*, n^* f^*), \tag{6}$$

where, $f^*(\boldsymbol{c}^*, r^*, z^*, t^*)$ is the velocity distribution function, $n^*(r^*, z^*, t^*)$ is the local number density, $\boldsymbol{c}^*$ is the velocity of a gas molecule and J is the bi-linear collision integral. The mean thermal speed of the gas molecules is $\langle c \rangle \equiv (8kT/(\pi m))^{1/2}$, where m is the mass of a gas molecule and T is the temperature of the gas. The Mach number, $M = U/\langle c \rangle$, is a measure of the deviation from equilibrium owing to the fluid velocity. Because the radial velocity of the gas in the lubrication gap is $O(UCa^{-1/4})$ and the pressure variations are $O(\sigma/a)$, the velocity distribution function, number density, temperature and mean free path variations due to the fluid flow are $O(MCa^{-1/4})$ and $O(\sigma/(ap_\infty))$. In practice, the criteria, $MCa^{-1/4} \ll 1$ and $\sigma/(ap_\infty) \ll 1$, are nearly always satisfied and we can linearize the velocity distribution function:

$$f^* = f^*_{MB}(1 + M\Xi), \tag{7}$$

where

$$f^*_{MB} = \left(\frac{m}{2\pi kT}\right)^{3/2} \exp\left(-\frac{mc^{*2}}{2kT}\right) \tag{8}$$

is the equilibrium Maxwell–Boltzmann distribution of velocities and $\Xi(\boldsymbol{c}^*, r^*, z^*)$ represents the deviation of the velocity distribution from equilibrium. Provided that $M \ll Ca^{1/4}$, we can solve a linearized quasi-steady equation for Ξ. This criterion is closely related to the criterion, $Re_g \ll Ca^{1/4}$ for neglecting inertial terms in the

equations of motion for continuum gas flow in a lubrication gap with gap thickness $aCa^{1/2}$.

We can derive the standard mass conservation equation,

$$\frac{\partial n^*}{\partial t^*} + \frac{1}{r^*}\frac{\partial}{\partial r^*}(r^* u_r^* n^*) + \frac{\partial}{\partial z^*}(u_z^* n^*) = 0, \tag{9}$$

by taking the zeroth moment of the Boltzmann equation. The variation of density in the mass conservation equation can be neglected when $MCa^{-1/4} \ll 1$ and $\sigma/(ap_\infty) \ll 1$ to yield the standard incompressible mass conservation equation. Integrating this equation across the lubrication gap and applying the boundary conditions (2) and (3) yields

$$\frac{\partial H^*}{\partial t^*} + \frac{1}{r^*}\frac{\partial}{\partial r^*}\left(r^* \int_{H_1^*}^{H_2^*} u_r^* \mathrm{d}z^*\right) = 0. \tag{10}$$

Although the effect of number density variations is negligible in the mass conservation equation, the number density (or pressure) variations drive a non-equilibrium velocity distribution function Ξ in the linearized Boltzmann equation that results in a mean velocity of the gas. It can be shown by scaling of the linearized Boltzmann equation that radial variations in p are more significant than axial variations, in analogy to the continuum lubrication problem. As a result, we can use existing solutions to the problem of rarefied gas flow driven by pressure gradients along a planar channel (the local geometry of the lubrication gap) to determine the relationship between the radial flux and the pressure gradient. This relationship can be expressed in the form

$$\int_{H_1^*}^{H_2^*} u_r^* \mathrm{d}z^* = \frac{2\phi(\delta)}{\pi\rho_g\langle c\rangle} H^{*2}\frac{\partial p^*}{\partial r^*}, \tag{11}$$

where ϕ is a non-dimensional function of a parameter, $\delta = H^*/\lambda = H\delta_{nc}$, which is the inverse of the Knudsen number based on the local gap thickness. Here, ρ_g is the ambient gas density far from the drop. Substituting (11) into (10) and non-dimensionalizing yields

$$W + \frac{\partial D}{\partial t} = \frac{2B}{\pi\delta_{nc}}\frac{1}{r}\frac{\partial}{\partial r}\left(r H^2 \phi(\delta)\frac{\partial p}{\partial r}\right), \tag{12}$$

where we have used the relationship $\mu_g = B\rho_g\langle c\rangle\lambda$. The exact value of B for hard sphere molecules is $5\pi/32$. However, in this analysis, we use the value $B = 1/2$, which leads to a an error of about 2% in the viscosity. This enables us to use the expression for the flux $\phi(\delta)$ or small δ derived by Sundararajakumar & Koch (1996). For $\delta > 10$, the effects of non-continuum flow may be approximated in terms of a Maxwell slip-boundary condition on the drop surfaces and

$$\phi = \frac{\pi}{12}\delta + 1.8 \quad \text{for} \quad \delta > 10. \tag{13}$$

This result is consistent with Hocking's (1973) analysis of lubrication flows between rigid spheres. The asymptotic result derived by Sundararajakumar & Koch (1996) for small δ is

$$\phi = \ln\left(\frac{1}{\delta}\right) + 0.4531 \quad \text{for} \quad \delta < 0.1. \tag{14}$$

When $0.1 < \delta < 10.0$, we use the results of a numerical solution of the Bhatnagar–Gross–Krook (BGK) approximation to the linearized Boltzmann equation presented

by Cercignani & Daneri (1963). The numerical values of Cercignani & Daneri are consistent with the analytical expressions in the limits of large and small δ.

The net surface deformation D obtained from a normal force balance is

$$\frac{1}{r}\frac{\partial}{\partial r}\left(r\frac{\partial D}{\partial r}\right) = \frac{1}{St^{1/2}}(p_\infty - p). \tag{15}$$

For $r \gg 1$, where the gap becomes large enough for a continuum approximation to hold, we find the asymptotic deformations to be of the form

$$D_i = -\frac{2}{3}\frac{\mathrm{d}W}{\mathrm{d}t}\ln r + c_i(t) + O\left(\frac{\ln r}{St^{1/2}r^2}\right) \quad \text{for} \quad i = 1, 2, \tag{16}$$

where the functions $c_1(t)$ and $c_2(t)$ are determined by matching the lubrication approximation to the outer solution. Equations (5), (12) and (15) indicate the relatively strong algebraic dependence of the pressure, deformation and drop velocity on St and δ_{nc}. An additional, weak logarithmic dependence on $We^{-1/4}$ arises from matching (16) with the outer solution. Here, $aWe^{1/4}$ is the maximum extent of the lubrication film region required before the kinetic energy of the drop is converted to energy of interfacial deformation.

We now turn to a consideration of the liquid flow and the deformation of the drop and interface outside the lubrication regime. These solutions will be matched with (16) to obtain the constants $c_1(t)$ and $c_2(t)$ and complete the determination of the lubrication problem. The liquid flow within the drop and the drop deformation outside the lubrication region can be obtained using the potential-flow analysis described by Gopinath & Koch (2001*a*). The velocity potential characterizing the flow field inside the drop and deformation in the outer region are written in series form using Legendre functions as basis functions. Matching this solution to (16) yields

$$c_2 = \frac{\mathrm{d}W}{\mathrm{d}t}\left[\tfrac{2}{3}\ln\left(\frac{Ca^{-1/4}}{N_c}\right) + 0.100\right] - \sum_{k=2}^{N_c} L_k, \tag{17}$$

where L_k and B_k are coefficients in the expansions for the deformation and velocity potential, which are determined from the ordinary differential equations:

$$\frac{\mathrm{d}L_k}{\mathrm{d}t} = kB_k \quad \text{for} \quad k \geqslant 2, \tag{18}$$

$$\frac{\mathrm{d}B_k}{\mathrm{d}t} = -\frac{2k+1}{3}\frac{\mathrm{d}W}{\mathrm{d}t} - (k^2 + k - 2)L_k, \tag{19}$$

with the initial condition that the coefficients are zero at the onset of the collision. The value of $c_2(t)$ is independent of the cutoff mode number N_c provided that N_c is sufficiently large.

To determine $c_1(t)$, we must analyse the flow and deformation in the half-space of liquid far from the drop, i.e the outer problem for the initially planar interface. The flow of the liquid far from the drop occurs over a length scale that is $O(a)$ and is governed by the Navier–Stokes equation. The gas pressure in the outer region is much smaller than the pressure induced in the liquid owing to the flow and can be ignored. Viscous effects in the liquid are small because the bounce time is short compared

with $\rho_l a^2/\mu_l$. The pressure in the liquid layer results primarily from the acceleration of the fluid. These observations lead us to consider inviscid equations of motion for the pressure p_1 and velocity $\boldsymbol{u}_1$ in the liquid layer:

$$\frac{\partial \boldsymbol{u}_1}{\partial t} = -\nabla p_1, \tag{20}$$

$$\boldsymbol{u}_1 = \nabla\phi, \tag{21}$$

$$\nabla^2\phi = 0. \tag{22}$$

Here, we scale the velocity potential with aU, the pressure with $\rho_l U^2 We^{-1/2}$, positions with a, time with the bounce time $aWe^{1/2}/U$, and the deformation with $aWe^{1/2}$.

Using the approximation that the $O(aWe^{1/2})$ deformation of the interface is small compared with the $O(a)$ wavelength, we can transform the kinematic and dynamic boundary conditions at the deformed interface into conditions applied at the undeformed interface $z' = 0$:

$$\left.\frac{\partial\phi_1}{\partial z'}\right|_{z'=0} = -\frac{\partial D_1}{\partial t}, \tag{23}$$

$$-\left.\frac{\partial\phi_1}{\partial t}\right|_{z'=0} + We^{-1/2}(p_\infty - p) = \frac{1}{r'}\frac{\partial}{\partial r'}\left(r'\frac{\partial D_1}{\partial r'}\right). \tag{24}$$

Taking the two-dimensional axisymmetric Fourier transform of (23) and (24) and expressing the velocity potential in terms of Fourier modes:

$$\phi_1(r', z', t) = 2\pi\int_0^\infty B(q, t)\mathrm{e}^{2\pi q r'} J_0(2\pi q r')q\,\mathrm{d}q, \tag{25}$$

where J_0 denotes the Bessel function of zero order, yields

$$-\frac{\partial\hat{D}_1}{\partial t} = 2\pi q B(q, t), \tag{26}$$

$$\frac{\partial B}{\partial t} - F = 4\pi^2 q^2 \hat{D}_1(q, t). \tag{27}$$

Here, the term $F = -(4\pi/3)\mathrm{d}W/\mathrm{d}t$ arises from the force exerted by the gas pressure in the lubrication gap on the interface. This force is treated as a delta function in space because the radial extent of the lubrication film is assumed to be much smaller than a. The constraint that the volume of the liquid layer does not change during the bounce yields $\hat{D}_1(q = 0, t) = 0$. The solution to (26) and (27) that satisfies causality and the condition of zero deformation and liquid velocity potential at $t = 0$ is:

$$\hat{D}_1(q, t) = -2\pi q\int_0^t F(t')\frac{\sin[\eta(t - t')]}{\eta}\mathrm{d}t', \tag{28}$$

where $\eta = (2\pi q)^{3/2}$. Taking the inverse transform of (28) in the limit of small r' and matching with the inner approximation to the deformation (16) for $r \gg 1$, the

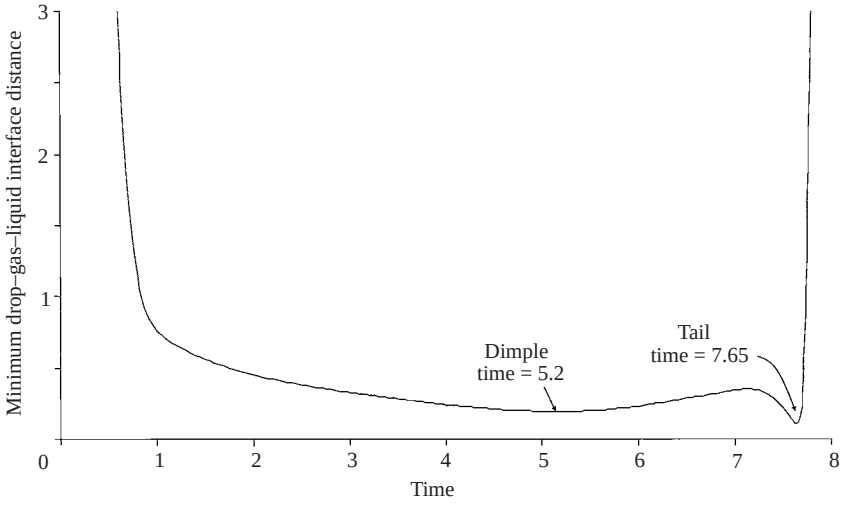

FIGURE 3. The minimum gap scaled with $aCa^{1/2}$ separating the drop and liquid layer is plotted as a function of time scaled with $aWe^{1/2}/U$ for $Oh = 2.4 \times 10^{-5}$ and $St^{1/2} = 25$.

matching constant is determined to be

$$c_1(t) = \frac{2}{3}\frac{\mathrm{d}W}{\mathrm{d}t}\left[\ln\left(\frac{Ca^{-1/4}}{\pi q_0}\right) - 0.5763\right] + 2\pi\int_0^{q_0} \hat{D}_1(q,t)q\,\mathrm{d}q, \tag{29}$$

where q_0 is a cutoff wavenumber satisfying $1 \ll q_0 \ll (2\pi r'_m)^{-1}$. Here, r'_m is a radial position in the matching region $We^{1/4} \ll r'_m \ll 1$. The matching constant is independent of the exact value of q_0 in the limit $We \ll 1$. Note the similarities between the matching condition for the interface (29) and the drop (17) deformation. In both cases, the sum over modes in the outer regions is cut off at a maximum value corresponding to the matching region and the exact results are independent of the cutoff parameter. The discrete sum in (17) is replaced by an integral in (29) because the interface is unbounded while the drop interface is finite.

We have seen that the parameters *St*, *We* and δ_{nc} that arise most naturally in the theory are different from those (*Kn*, *Oh* and *We*) that are most convenient for describing the experiments. Thus, we will first express the theoretical results in terms of *St*, *We* and δ_{nc} and then convert them to the experimental parameters when comparing with the measurements.

The dynamics of a drop–interface collision are illustrated in figures 3 to 7 for a drop with $St^{1/2} = 25$ and $We = 2.25 \times 10^{-4}$ in a continuum gas. This Stokes number is typical of the conditions encountered in the experiments. For example, it is equal to the Stokes number for the transition from coalescence to bouncing for the smaller drops in methane at the higher gas pressure. On the other hand, the Weber number is two or three orders of magnitude smaller than the values probed by the experiments. The matching between the inner and outer approximations to the drop shape requires $We^{-1/4} \ll 1$ to provide a clear separation of length scales between the radius of the thin-film region and the radius of the drop. In practice, the numerical method is only stable for *We* smaller than about 10^{-3}. Therefore, to make a quantitative comparison with the experimental measurements in the following two sections, it will be necessary to extrapolate the results of the theoretical calculations to the higher values of *We* investigated experimentally.

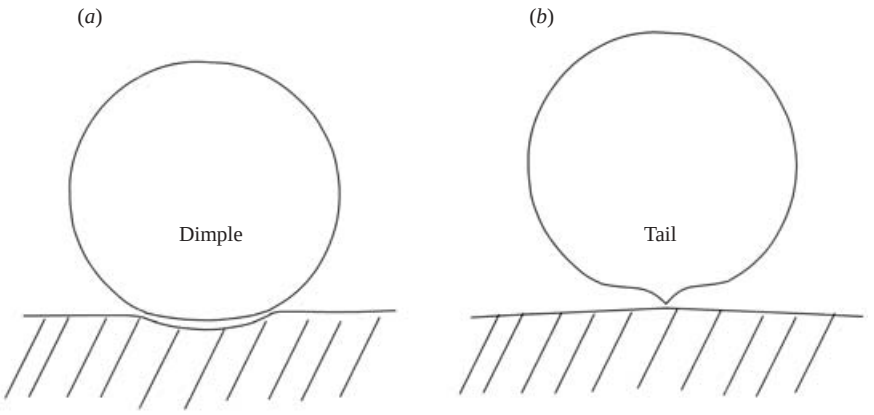

FIGURE 4. Qualitative sketch of the drop shapes that occur during the collision.

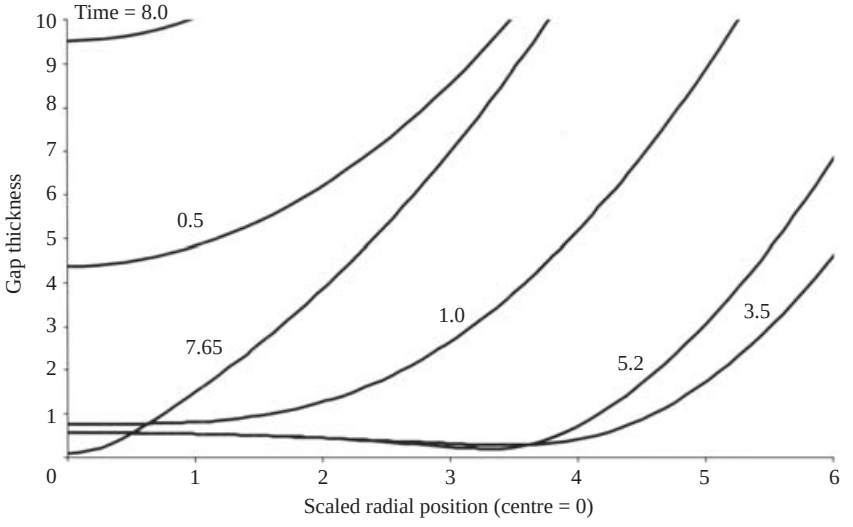

FIGURE 5. Profile of gap thickness as a function of radial position at several times during the collision for $Oh = 2.4 \times 10^{-5}$ and $St^{1/2} = 25$. The gap thickness, radial position and time are scaled with $aCa^{1/2}$, $aCa^{1/4}$ and $aWe^{1/2}/U$, respectively.

The minimum gap separating the drop and liquid layer is plotted as a function of time in figure 3. The minimum gap thickness is an important feature to consider since it is the most likely site for coalescence to occur. The drop and interface begin to deform and the rate of thinning of the lubrication film slows dramatically when the gap non-dimensionalized by $aCa^{-1/2}$ is approximately 1. However, as the deformation proceeds the gap thickness becomes much smaller than 1. The high Stokes number of the collision implies that the radial extent of the lubrication region must become large to generate a force sufficient to reverse the momentum of the drop. To sustain the elevated pressure required to maintain this deformed region over an extended period of time, the gap thickness must become small. This allows an $O(\sigma/a)$ pressure to be maintained despite a small outflux of gas. A qualitative sketch of the drop shapes that occur during the collision is given in figure 4, the profiles of gap thickness and

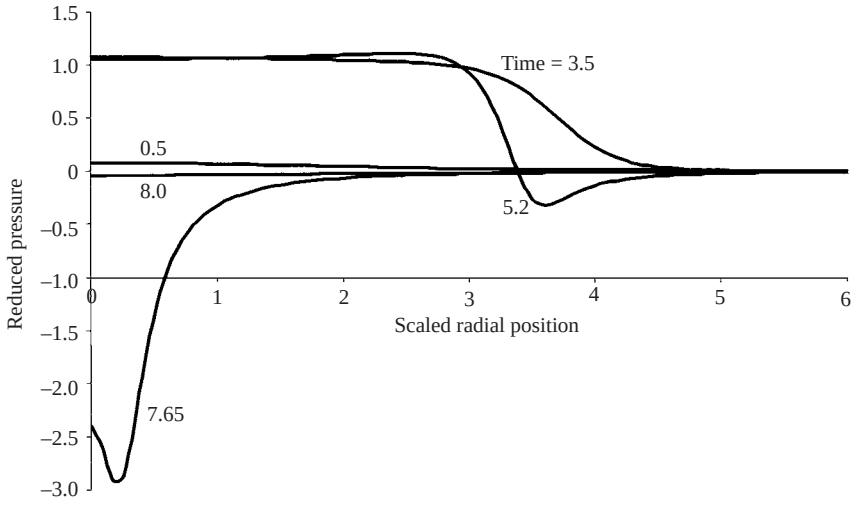

FIGURE 6. Profile of gas pressure as a function of radial position at several times during the collision for $Oh = 2.4 \times 10^{-5}$ and $St^{1/2} = 25$. The pressure, radial position and time are scaled with σ/a, $aCa^{1/4}$ and $aWe^{1/2}/U$, respectively.

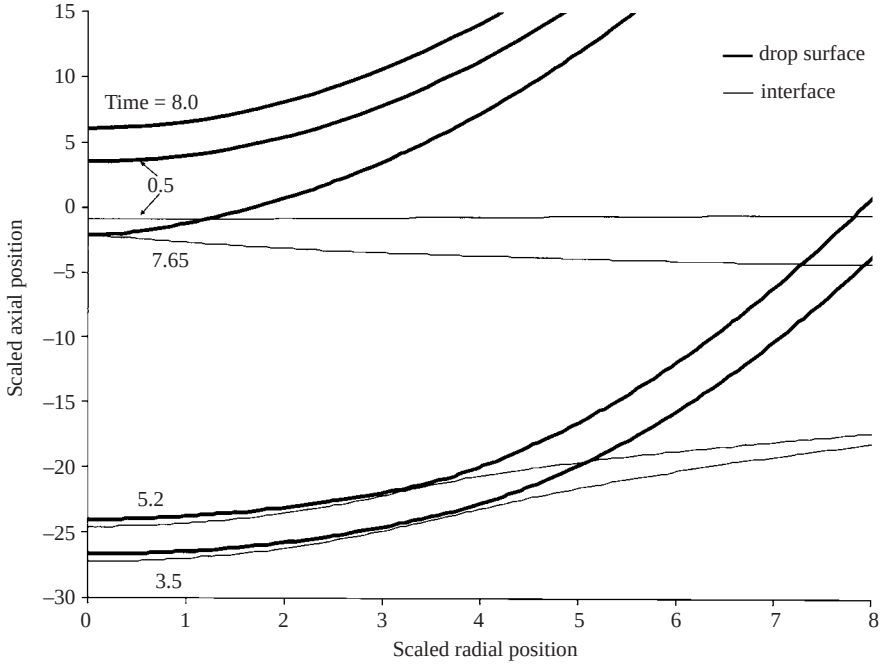

FIGURE 7. Shapes of the drop and liquid interfaces at several times for $Oh = 2.4 \times 10^{-5}$ and $St^{1/2} = 25$. The interface position, radial position and time are scaled with $aCa^{1/2}$, $aCa^{1/4}$, and $aWe^{1/2}/U$, respectively.

gas pressure as functions of radial position for several times during the collision are plotted in figures 5 and 6, respectively. Figure 7 presents the shapes of the drop and liquid interfaces at several times. When the dimensionless gap thickness thins to about 1 at $t = 1$, the gap thickness profile (figure 5) begins to flatten. The flat region

spreads outward until about $t = 3.5$ and then begins to retract inward. The actual drop and interface shapes during this time period are illustrated by the first drawing in figure 4. In the thin-gap region, the two interfaces are nearly parallel and have a radius of curvature that is twice the radius of the drop. This result can be rationalized easily if we recognize that two curved fluid interfaces are available to accomplish the change in reduced pressure from $2\sigma/a$ in the drop to 0 in the liquid layer below. Close examination of the profiles in figures 5 and 7 indicates that the interfaces for $t = 3.5$ and 5.2 are not exactly parallel. Instead, the gap is thinner at the rim of the film. We will refer to this shape as a dimple as it arises owing to the same mechanism that leads to a concave dimple shape in drop–drop collisions (Gopinath & Koch 2001*a*). The thin film at the rim allows the pressure to drop rapidly from a value near σ/a required to maintain the reduced curvature of the film region to 0. (See the pressure profiles for $t = 3.5$ and 5.2 in figure 6.) The minimum gap thickness occurs slightly later ($t = 5.2$) than the maximum radial extent of the dimple ($t = 3.5$) because of the smaller amount of gas available to maintain the pressure drop at longer times. As the drop recedes from the surface and the dimple relaxes, a region in which the pressure is smaller than ambient arises outside the dimple where the drop and interface are peeling away from one another. The amplitude of this pressure valley increases with time and becomes large when the dimple vanishes. Some of the energy of drop deformation is released to form a relatively sharp tail in the drop, as illustrated in figure 4(*b*). This leads to a second minimum in the profile of drop–interface separation versus time (figure 3). The tail consists of a very sharp decrease in gap thickness with decreasing radial position, as illustrated in figure 5 for $t = 7.65$. These profiles arise from both a tail in the drop and a rise in the gas–liquid interface near the centreline, as seen in figure 7.

4. Coalescence–bounce transition

In this section, we compare theoretical and experimental results for the transition between drop coalescence and drop bouncing. We consider first collisions of a drop with an initially planar interface. As we noted in § 3, the parameters that appear naturally in the theory are δ_{nc}, the ratio of the gap thickness $aCa^{1/2}$ at which the interfaces first start to deform to the mean free path of the gas, $St^{1/2}$, the ratio of the amplitude of interfacial deformation to the film thickness, and $\ln(We^{-1/4})$, the logarithm of the ratio of the drop radius to the maximum radial extent of the thin-film region. Thus, we performed computations to determine the critical value of δ_{nc} above which drops bounce for a range of values of $St^{1/2}$ and $\ln(We^{-1/4})$. For each [$St^{1/2}$, $\ln(We^{-1/4})$] pair, we computed the minimum gap thickness achieved during the bounce process as a function of δ_{nc}. For values of δ_{nc} sufficiently close to the transition, the minimum gap was a linear function of δ_{nc}. The intersection of this line with zero minimum gap was taken as the critical δ_{nc}. For all the parameter values considered here, the minimum gap thickness corresponding to the tail approached zero, leading to coalescence, while the minimum gap during the dimple stage remained finite. The resulting critical δ_{nc} values (solid symbols) are plotted as a function of $\ln(We^{-1/4})$ for several values of $St^{1/2}$ in figure 8. A good fit to the data for $St^{1/2} = 17.5$, 24.2 and 37 is given by

$$\delta_{nc} = 8.09 - 0.254St^{1/2} + 0.0088St + 0.582\ln\left(We^{-1/4}\right) + 0.102St^{1/2}\ln\left(We^{-1/4}\right). \quad (30)$$

Because $St^{1/2} = 50$ is near the upper limit for which accurate computations can be performed, we did not use the calculations at this Stokes number to establish the

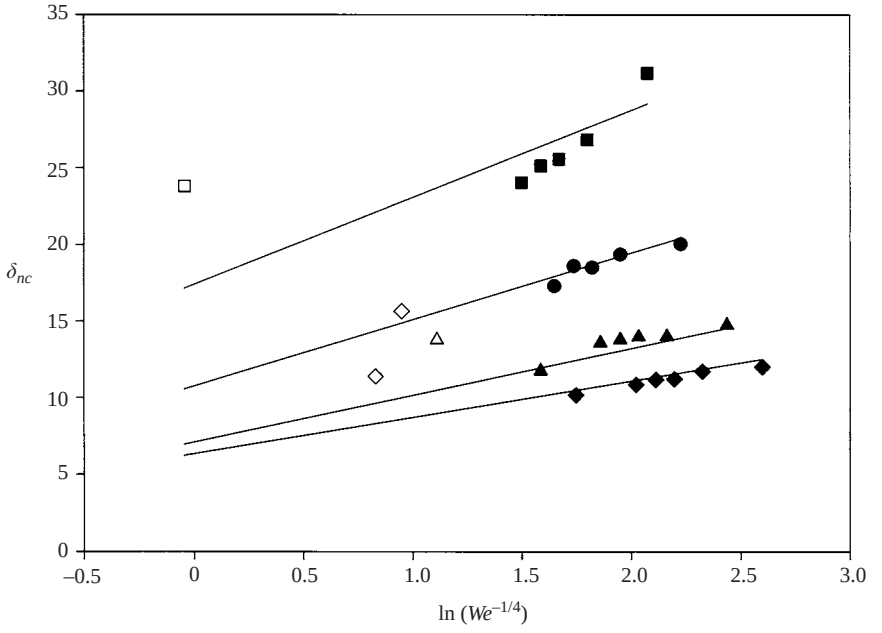

FIGURE 8. The critical value of δ_{nc} above which a drop bounces from a gas–liquid interface is plotted as a function of $\ln(We^{-1/4})$ for $St^{1/2} = 17.5$ (lowest line and diamonds), 24.2 (next lowest line and triangles), 35 (third line and circles), and 50 (highest line and filled squares), and 54 (open square). The filled symbols are numerical simulations, the lines are the fit (30) to the simulation data, and the open symbols are experimental measurements.

fit. However, the values of δ_{nc} given by (30) are in reasonable agreement with the computations at $St^{1/2} = 50$.

The computations covered most of the range of Stokes numbers obtained in the experiments described in § 2. However, the transitional Weber numbers in the experiments were $O(0.1–1)$ whereas the highest value of We for which stable computations could be performed was about 10^{-3}. As a result, it is necessary to extrapolate the computational results to higher Weber numbers to compare with the experiments. Fortunately, the dependence of the critical condition on We is only logarithmic. The experimental measurements that correspond to the Stokes numbers for which the computations were performed are plotted as the open symbols in figure 8. It can be seen that the experimentally determined values of the critical δ_{nc} are similar in magnitude to the extrapolation, (30), of the theoretically determined critical δ_{nc}.

A more complete comparison of the theory, (30), with all of the experimentally determined coalescence–bounce transitions for drop–interface collisions is given in figure 9. In this figure, the results are presented in terms of the most convenient experimental parameters. The critical Weber number above which the drop bounces is plotted as a function of the Ohnesorge number for two values of the Knudsen number. The upper curve and squares correspond to the predictions and experiments for $Kn \approx 6.9 \times 10^{-4}$ and the lower curve and diamonds to predictions and experimental results for $Kn \approx 5.5 \times 10^{-4}$. The Knudsen number was varied in the experiments by changing the gas pressure. It can be seen that the theory and experiments indicate a similar downward shift in the Weber number for the coalescence–bounce transition with decreasing Kn (increasing pressure). The Ohnesorge number was varied by

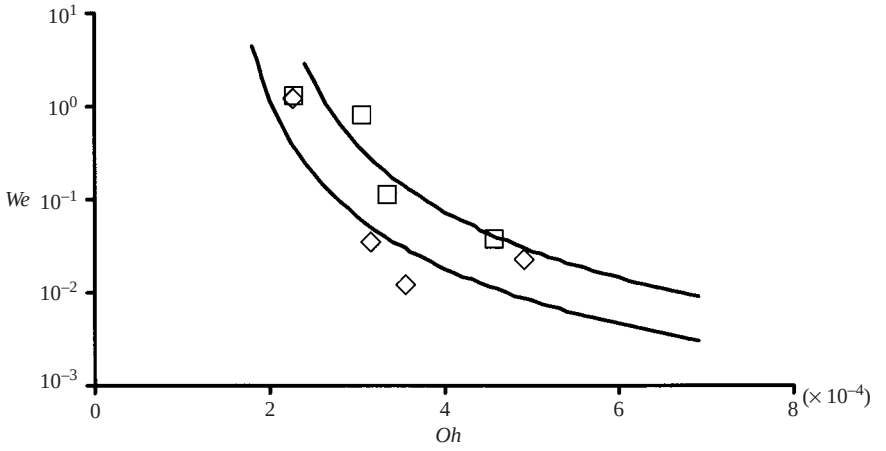

FIGURE 9. The critical Weber number above which drops bounce from a gas–liquid interface is plotted as a function of the Ohnesorge number. The lines are the fit (30) to the theoretical results and the symbols are experimental measurements. The lower line and diamonds are for $Kn \approx 5.5 \times 10^{-4}$, while the upper line and squares are for $Kn \approx 6.9 \times 10^{-4}$.

changing the gas viscosity (using methane or nitrogen) and by varying the drop radius. Both theory and experiment indicate a sharp decrease in the critical Weber number with increasing *Oh*. Note that the critical Weber number is a very strong function of both *Kn* and *Oh*, indicating that there exists only a narrow range of (*Kn*,*Oh*) values for which a transition is observed for realistic values of *We*. In other words, only special choices of the gas pressure, gas and liquid composition and drop size will lead to an observed transition as the drop velocity is varied. This theoretical prediction is consistent with our experience in conducting the experiments.

Coalescence can result either from the diminution of the viscous resistance of the gas due to non-continuum effects or from van der Waals forces. The relative importance of these two effects is described by a parameter $\alpha = h^*_{vdW}/(5\lambda)$, which is the ratio of the gap thickness $h^*_{vdw} = (6\pi\sigma/Aa)^{1/3}$ at which the pressure due to van der Waals forces is equal to the Laplace pressure σ/a to the gap thickness 5λ at which the lubrication pressure between two colliding spheres is reduced to half its continuum value (Sundararajakumar & Koch 1996). In our experimental study, $\alpha = 0.083$–0.17, indicating that non-continuum effects arise well before van der Waals forces as the gap thins. As a result, we expect that van der Waals forces have only a minor influence on the transition from coalescence to bouncing for normal collisions of small-Weber-number aerosol drops. It may also be noted that there is no correlation between the deviations of the experimental measurements in figure 9 from the theory and the value of α.

A direct comparison of our theory with the previous experiments of Jayaratne & Mason (1964) is not possible because of the oblique geometry of the collisions in those experiments. However, extrapolating Jayaratne & Mason's results for the critical velocity for 74 μm radius drops, we estimate the critical velocity for normal incidence would be about 51 cm s^{-1} corresponding to $We = 0.27$. For this Weber number and the experimental Ohnesorge number, $Oh = 2.27 \times 10^{-4}$, (30) predicts a critical Knudsen number of 6.1×10^{-4} which is similar to the experimental value $Kn = 7.9 \times 10^{-4}$. For the larger drops considered by Jayaratne & Mason, it is either difficult to obtain a reasonable extrapolation to normal incidence or the Weber number is large. However,

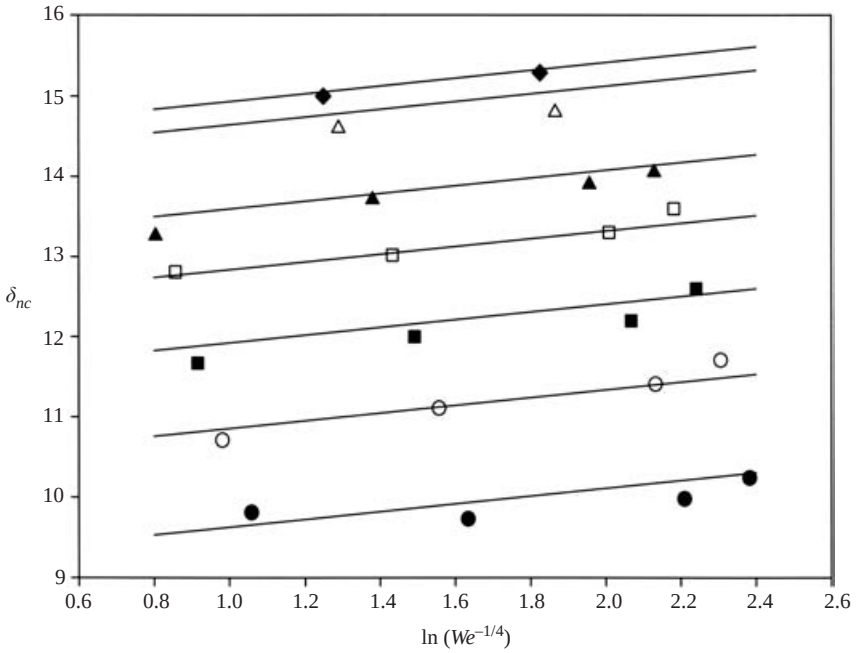

FIGURE 10. The critical value of δ_{nc} above which two drops bounce is plotted as a function of $\ln(We^{-1/4})$ for (from bottom to top) $St^{1/2} = 12$, 14, 16, 18, 20, 24 and 26. The symbols are results of numerical simulations and the lines are the fit, (31).

their experiments show that the critical Weber number decreases with increasing drop size at constant gas pressure. This trend is in agreement with our experiments and theory.

Next, we consider the transition from coalescence to bouncing for the collision of two equal-sized drops with a relative velocity $2U$ along their line-of-centres. The calculations are performed by incorporating a non-continuum flux, similar to that described in § 3, into the description of drop–drop collisions described by Gopinath & Koch (2001*a*). The critical value of δ_{nc} is determined for various values of $St^{1/2}$ and $\ln(We^{-1/4})$ using the procedure described above for drop–interface collisions. For drop–drop collisions like drop–interface collisions, the coalescence occurs during the tail formation after the centres of mass of the drops have started to recede from one another. The critical values of δ_{nc} determined from the computations are plotted as symbols in figure 10 for $St^{1/2} = 12$–26 and $We \approx 10^{-4}$–10^{-2}. The lines indicate the fit

$$\delta_{nc} = -1.49 + 1.12St^{1/2} - 0.0195St + 0.484 \ln\left(We^{-1/4}\right). \tag{31}$$

The results for the transition from coalescence to bouncing for the collision of two drops are similar to those for a drop–interface collision. For example, at $St^{1/2} = 18$ and $\ln(We^{-1/4}) = 2$, the critical value of δ_{nc} is 13.3 for a drop–drop collision and 11.2 for a drop–interface collision. The critical value of δ_{nc} is slightly smaller for the drop–interface collision, indicating that drops bounce more easily from an interface than from a second equal-sized drop. The critical δ_{nc} for the drop–interface collision has a stronger dependence on the Weber number such that the difference in the critical conditions for drop–interface and drop–drop collisions grows with increasing We. The greater stability of the drop–interface system and the stronger dependence

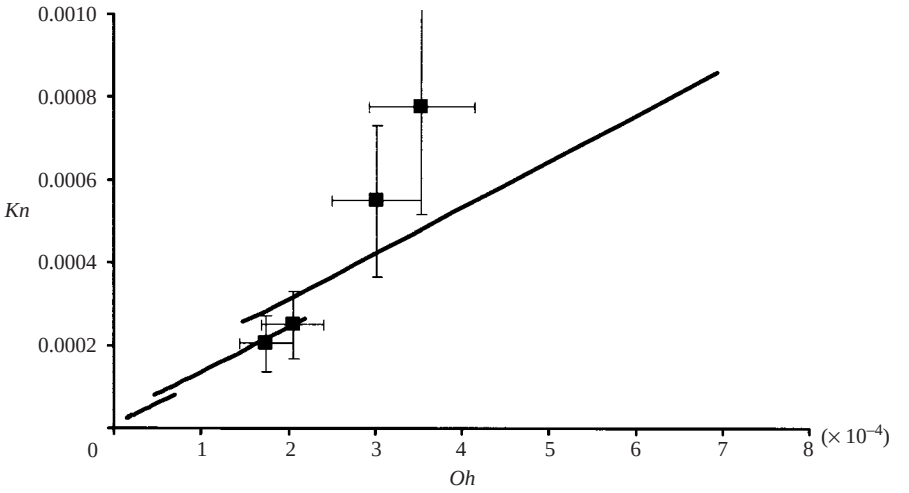

FIGURE 11. The critical Knudsen number above which two drops coalescence on impact is plotted as a function of the Ohnesorge number. The lines correspond to the fit, (31), to the theoretical results for (from bottom to top) $We = 10^{-4}$, 10^{-3} and 10^{-2}. The squares are the experimental results of Qian & Law (1997). The vertical and horizontal error bars indicate the uncertainty in the values of Kn and Oh resulting from the fact that a range of drop radii were used in the experiments.

on $\ln(We^{-1/4})$ arise because an initially planar interface is more easily deformed by the pressure developed in the lubrication gap than an initially spherical drop. The deformation of the interface allows the lubrication gap to remain finite preventing coalescence under conditions where two drops would coalesce.

The theoretical results, (31), for the drop–drop transition are presented as solid lines in figure 11 in terms of the dimensionless variables (Kn, Oh, We) that are most convenient for an experimental study. The critical Knudsen number is plotted as a function of Oh for three values of We and the results cover the range of Oh and We explored in the numerical simulations. It can be seen that the dependence of the critical Knudsen number on the Weber number is very weak, while the critical Knudsen number grows rapidly with increasing Oh. Thus, the bounce–coalescence transition for two drops like that for a drop and an interface is most sensitive to the drop radius, gas pressure, gas viscosity, liquid density and interfacial tension and has a weak dependence on the impact velocity.

Qian & Law (1997) observed oblique collisions between two equal sized drops with radii of 100–200 μm. The relatively large size of the drops led to Weber ($We = 5$–20) and Stokes numbers ($St^{1/2} = 70$–170) that are considerably larger than those explored in our theoretical study. Thus, the assumption of small-amplitude drop deformation is not appropriate to Qian & Law's study. Nonetheless, there are similarities in the qualitative trends revealed by these experiments and those predicted by the present theory. For example, Qian & Law observed that hydrocarbon drops with lower surface tension bounce more readily than water drops. Lower surface tension gives higher We and Oh both of which promote bouncing, according to the theory. In addition, Qian & Law noted that drops bounce more readily in 7.5 atm helium than in 1 atm nitrogen. The primary difference between these gases is the smaller mean free path and Knudsen number in the high-pressure helium. The theory predicts a strong influence of Knudsen number on the critical Weber number.

Qian & Law (1997) present maps of the collision regimes (bouncing, coalescence, or coalescence followed by break up) as a function of the Weber number and the angle between the relative velocity and the line-of-centres. Results were reported for collisions between two water drops and two hydrocarbon (*n*-tetradecane) drops in nitrogen and helium atmospheres. For each liquid–gas pair, the collision regime map is given for three different pressures: a low pressure at which nearly head-on collisions at moderately small *We* ($We < \sim 40$) lead to coalescence, a high pressure at which normal collisions at moderately small *We* lead to bouncing, and an intermediate pressure at which a transition from coalescence to bouncing is observed at $We = 5$–20. Since the experiments involved oblique collisions, the results for normal collisions are obtained by extrapolation. From our theoretical and experimental studies, we believe that the range of pressures for which the intermediate coalescence regime map is observable is relatively narrow. In figure 11, we plot the Knudsen numbers (squares) corresponding to the gas pressures for which Qian & Law observe transitions from coalescence to bouncing for head-on collisions for the four different gas–liquid pairs. The error bars indicate the uncertainty resulting from the fact that Qian & Law plot data for a range of drop radii on a single graph. The critical Knudsen numbers in Qian & Law's experiments have a similar magnitude to those predicted by the theory for the same Ohnesorge number. Although the Weber number in the experiments is different from that for which theoretical calculations have been performed, the predicted dependence of the critical *Kn* on *We* is weak, at least in the regime $We \ll 1$. The experiments and theory both indicate an increase of the critical *Kn* with increasing *Oh*.

A striking result of the present study is that the transition from coalescence to bouncing for slightly deformable aerosol droplets is only weakly dependent on the Weber number or impact velocity. It is interesting to contrast this situation with the behaviour of slightly deformable drops suspended in a viscous liquid (Rother, Zinchenko & Davis 1997) and highly deformed drops (Qian & Law 1997). When two sedimenting drops undergo an oblique collision in a viscous liquid, interfacial deformation occurs at a larger gap thickness when the capillary number (or velocity) is increased. As a result, increasing relative velocity prevents coalescence. The deformation of aerosol drops also begins at larger gap thicknesses when the capillary number (velocity) is increased. However, the amplitude of interfacial deformation required to produce a bounce increases with increasing Weber number (velocity) and the minimum gap thickness decreases throughout the bounce process. As a result, the minimum gap thickness and tendency for coalescence between small aerosol drops is weakly dependent on the impact velocity.

Aerosol drops undergoing normal collisions can experience a transition from coalescence to bouncing at small to moderate *We* followed by a transition from bouncing to coalescence at higher Weber numbers, $We \approx 80$–160. The first transition has been the focus of the present contribution. Qian & Law (1997) observed both transitions in their experiments and developed a simple model for the high *We* transition. At high *We*, the time of contact between two drops increases with increasing *We* thereby allowing a longer time for the gas film between the drops to thin. This leads to a strong dependence of this second transition on *We* and a tendency for large velocities to promote coalescence. In the limit $We \ll 1$, the bounce time $t_b = (\rho_l a^3/\sigma)^{1/2}$ is independent of the impact velocity and this results in a weak dependence of the first coalescence–bounce transition for small droplets on the impact velocity.

In our theoretical studies, we found that the two liquid–gas interfaces approach one another and form a very small gap first at the rim of the lubrication film as a dimple forms and subsequently at the centre of the lubrication film as a tail forms

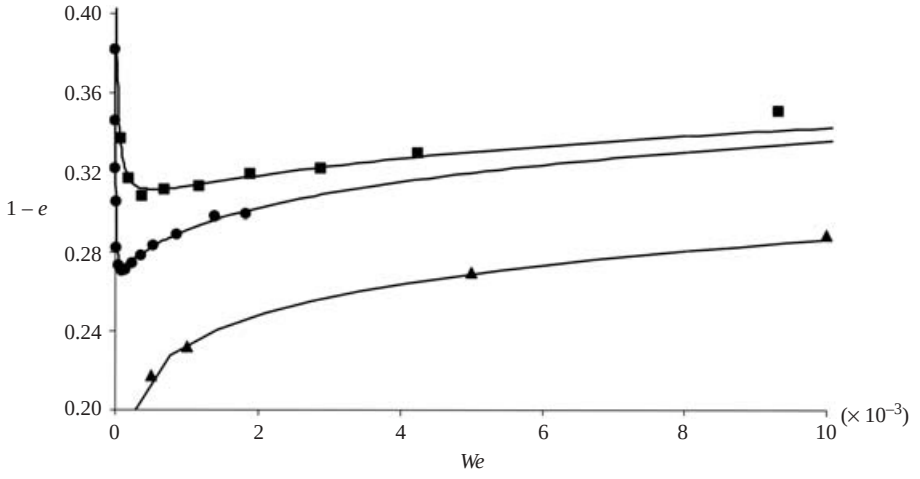

FIGURE 12. The computed coefficients of restitution for for drop–interface collisions for two Ohnesorge numbers, 7.6×10^{-6} (circles) and 2.15×10^{-5} (squares) plotted as a function of Weber number. The triangles are for a repulsive force separating the drop and fluid layer and corresponds to $Oh = 0$. The lines are the fit, (33).

in the receding drop(s). This phenomenon is illustrated in figures 3, 4 and 5 for a drop–liquid-layer collision, but also applies to drop–drop collisions. If the gas film at the rim became small enough compared with the mean free path, then coalescence could occur there first, leading to trapping of a bubble. If coalescence does not occur at the rim, it could subsequently occur by the two tails touching as the drop(s) recede. In our theoretical studies of drop–drop and drop–interface collisions for $We \ll 1$, we always found that coalescence occurred at the tail at the critical Weber number for transition from coalescence to bouncing. In an experimental study of the impact of large drops ($a > \sim 1.5$ mm) with $We > 6$, Thoroddsen, Etoh & Takehara (2003) observed coalescence at the rim. It is conceivable that there is transition from tail coalescence to rim coalescence with increasing *We*. It should also be noted, however, that our prediction only applies to the point of transition, whereas Thoroddsen *et al.*'s experiments were not conducted near a critical *We*. Since the minimum gap at the rim occurs earlier than that at the centre (figure 3), it is to be expected that there would be a transition from tail coalescence to rim coalescence as we move away from the critical *We*.

5. Coefficient of restitution

During the bounce of a drop with a gas–liquid interface, part of the drop's kinetic energy is stored as interfacial deformation energy and then restored to kinetic energy of drop translation after the bounce. However, a portion of the energy is used to create drop oscillations and waves on the gas–liquid interface. In addition, some of the energy is dissipated by the viscous flow in the gas film. The energy lost to oscillations of the interfaces in the absence of viscous dissipation can be computed using the model in which the drops and interface are prevented from coalescing by a repulsive force and no effect of the viscous stress in the gas is included. This result is indicated by the triangles in figure 12 and can be fit by the power law

$$1 - e = 0.432\ We^{0.0896}, \tag{32}$$

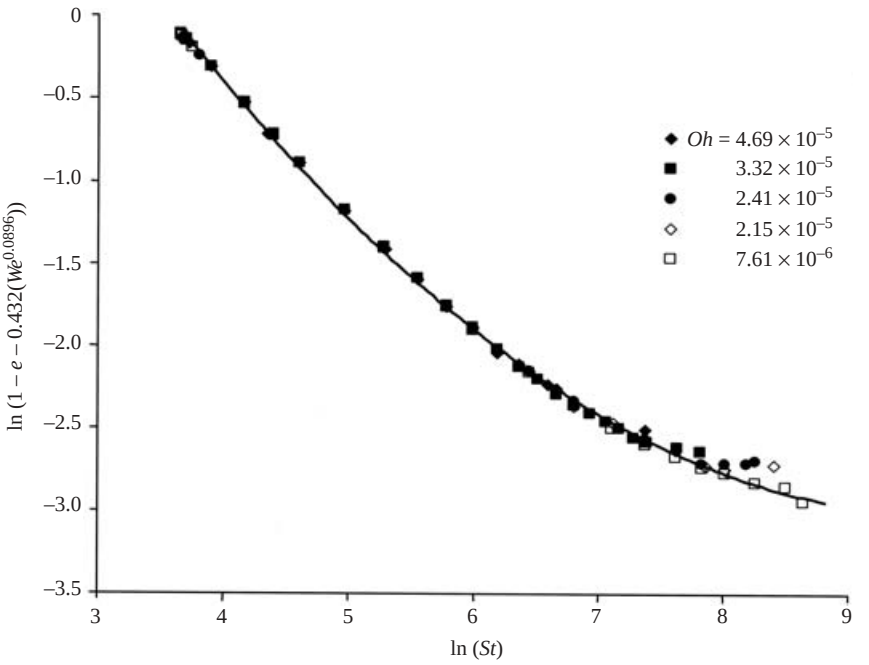

FIGURE 13. The viscous dissipation contribution to the coefficient of restitution of a drop colliding with a gas–liqud interface, i.e. $1-e-0.432\,We^{0.0896}$, is plotted as a function of $\ln(St)$. The symbols represent computational results for a range of Ohnesorge numbers and the line is the fit given by (33).

where e is the coefficient of restitution defined as the ratio of the velocity after collision to the velocity before collision. The energy lost to surface waves increases with increasing Weber number owing to the increased amplitude of the interfacial deformation.

When the effect of the gas film on the drop bounce is considered, we find that the coefficient of restitution is insensitive to the mean free path of the gas except at conditions very close to the coalescence–bounce transition. Consistent with this prediction, we found no dependence of the experimentally observed coefficients of restitution on the gas pressure. Thus, we will present theoretical results for the coefficient of restitution based on continuum lubrication forces in the gas film. The computed coefficients of restitution for two Ohnesorge numbers, 7.6×10^{-6} (circles) and 2.15×10^{-5} (squares) are plotted as functions of Weber number in figure 12. The coefficient of restitution is low at small Weber numbers where the Stokes number is relatively small. (Note that $St=We^{1/2}/Oh$.) The Stokes number is the ratio of the inertia of the drop to the gas viscosity, so, the lower the Stokes number, the more readily the gas viscosity can dissipate the kinetic energy of the liquid motion. As the Weber number is increased, e passes through a maximum and then decreases owing to the increasing importance of losses to surface oscillations. We performed calculations for a range of Ohnesorge numbers from 7.6×10^{-6} to 4.69×10^{-5} and Stokes numbers from 40 to 5000 and found that the difference between the coefficient of restitution and the value given by (9) for $Oh=0$ was only a function of the Stokes number. This is demonstrated in figure 13. The coefficient of restitution for finite Oh can be fitted well by

$$1-e=0.432\,We^{0.0896}+87.3\,St^{-1.53}\exp\{0.0783[\ln(St)]^2\}. \tag{33}$$

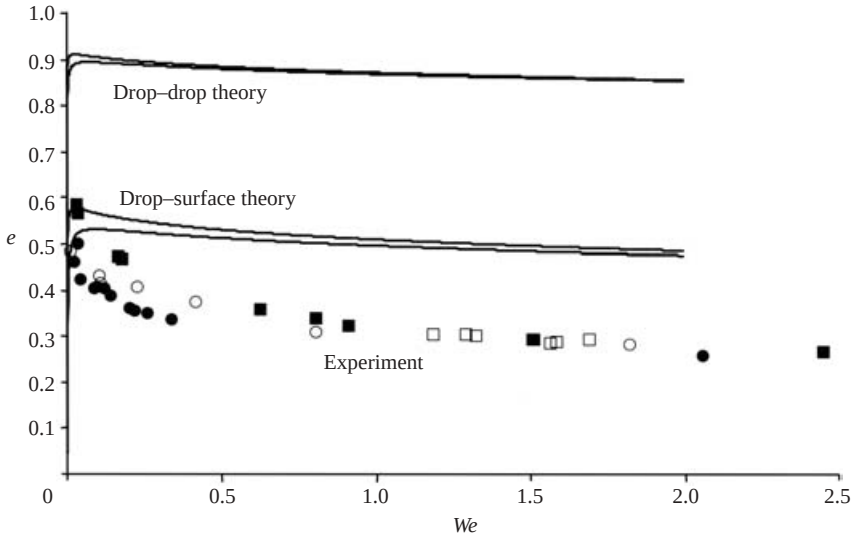

FIGURE 14. Experimental measurements for the coefficient of restitution of a drop colliding with a gas–liquid interface along with the predictions (33) and (34) for drop–interface and drop–drop collisions corresponding to the lowest (2.3×10^{-4}) and highest (4.9×10^{-4}) values of the Ohnesorge number in the experiments. In each case, the higher *Oh* value yields the lower of the two curves. The circles and squares are the experiments with nitrogen and methane, respectively. The closed symbols are for the smaller drops and the open symbols for the larger drops.

This fit is indicated by the lines in figure 12 and it reproduces the full dependence of e on We at various values of Oh. We conducted a similar series of calculations for drop–drop collisions and found the coefficient of restitution to be fitted well by

$$1 - e = 0.1\, We^{0.22} + 49\, St^{-1.71} \exp\{0.0971[\ln(St)]^2\}. \tag{34}$$

The experimental measurements for the coefficient of restitution are plotted in figure 14 along with the predictions (33) and (34) for drop–interface and drop–drop collisions corresponding to the lowest (2.3×10^{-4}) and highest (4.9×10^{-4}) values of the Ohnesorge number in the experiments. Both experiments and theory for drop–interface collisions yield a significantly lower coefficient of restitution than is predicted for drop–drop collisions. The initially planar gas–liquid surface is more readily deformed than a spherical drop in which the volume of the liquid is constrained. As a result, more energy is lost to surface waves in the drop–interface collisions than is lost to oscillatory modes in the drop–drop collisions. The continuum theory predicts a peak in the coefficient of restitution at $We = 0.025$ for $Oh = 2.3 \times 10^{-4}$ and $We = 0.09$ for $Oh = 4.9 \times 10^{-4}$. This peak typically occurs near the critical Weber number for the coalescence–bounce transition for the gas pressures studied here. Thus, our experimental measurements are primarily after the peak and indicate the downward trend of the coefficient of restitution with Weber number resulting from the increasing importance of energy loss to surface oscillations. The qualitative trends of the coefficient of restitution are similar for the theory and experiment. In particular, the coefficient of restitution decreases with increasing We and increasing Oh and the effect of Oh diminishes with increasing We. However, the absolute values of the measured coefficients of restitution are about 0.2 smaller than the predictions and the observed variation of e with We and Oh is larger than predicted. For example, the difference

between the coefficient of restitution predicted for the highest and lowest Oh at $We = 0.1$ is 0.034 whereas the variation among the experimental measurements is about 0.09. The experimental coefficients of restitution decrease by about 0.2 with increasing Weber number, while the predictions decrease by about 0.1.

One reason for the lower energy loss predicted by the theory could be the neglect of viscous dissipation due to the flow in the liquid. To investigate this possibility, we performed a calculation with a repulsive force replacing the gas film, but including the effects of viscous dissipation in the drop and the liquid sublayer. This calculation is similar to that outlined in § 2.4.2 of Gopinath & Koch (2001*a*) for drop–drop collisions. We found that viscous dissipation in the liquid lowered the coefficient of restitution by only 0.01 at $We = 0.1$ and $Oh_l = \mu_l/(\rho_l a\sigma)^{1/2} = 0.0189$. The energy lost to viscous dissipation in the liquid is proportional to the liquid Ohnesorge number Oh_l for $Oh_l \ll 1$ and decreases with decreasing We. The value of Oh_l chosen for this sample calculation corresponds to water drops of radius 40 μm. Marangoni stresses associated with contamination of the gas–water interface by surfactants would be another possible reason for the smaller coefficient of restitution observed in the experiments. However, we believe that such an effect would lead to a considerable variation in the measured coefficient of restitution from one experimental trial to the next and this was not observed. Since the difference between theory and experiment remains at higher We when the effect of viscous dissipation in the gas film becomes negligible, we do not believe that it arises from errors in the detailed treatment of the gas flow in the lubrication regime. We postulate instead that errors associated with the assumption of small-amplitude deformation (valid for $We^{1/2} \ll 1$) and the matching of inner and outer solutions (valid for $We^{1/4} \ll 1$) restrict the range of quantitative accuracy of the theory to $We < 10^{-4}$, which is smaller than the experimental Weber numbers (0.01 to 2). It would therefore be valuable to develop a numerical method that is capable of including non-continuum effects in the thin gap between the drop and interface while simultaneously resolving the full nonlinear deformation of the interfaces. Nobari *et al.* (1996) used a finite-difference method to simulate drop–drop collisions and determine the coefficient of restitution for large Weber number drops ($We = 50$–450). They observed the qualitative trends of decreasing coefficient of restitution with increasing drop deformation (increasing Weber number) and increasing viscosity (decreasing Reynolds number). However, they did not investigate slightly or moderately deformable drops and did not resolve the gas film down to the very small gap thicknesses that play a role in determining the viscous losses in low We drop collisions.

6. Drop formation following coalescence

After a drop coalesced at the interface, we observed the emission of a new, smaller (daughter) drop. A sample trajectory showing the formation of a daughter drop is presented in figure 15. The mother drop approaches the interface, bounces, returns to the interface and coalesces. Thereafter, a smaller drop is emitted with a velocity that is higher than the incident velocity of the mother drop. The fact that the new drop is smaller can be discerned easily by noting that the velocity of the new drop after it reaches its peak height and approaches terminal velocity is lower than the corresponding velocity of the mother drop after its bounce. In the example shown here, the mother bounced once before coalescing. However, in many of our studies (especially those at relatively small gas pressures), the mother coalesced on the initial impact and this enabled us to vary the impact velocity of the mother over a significant

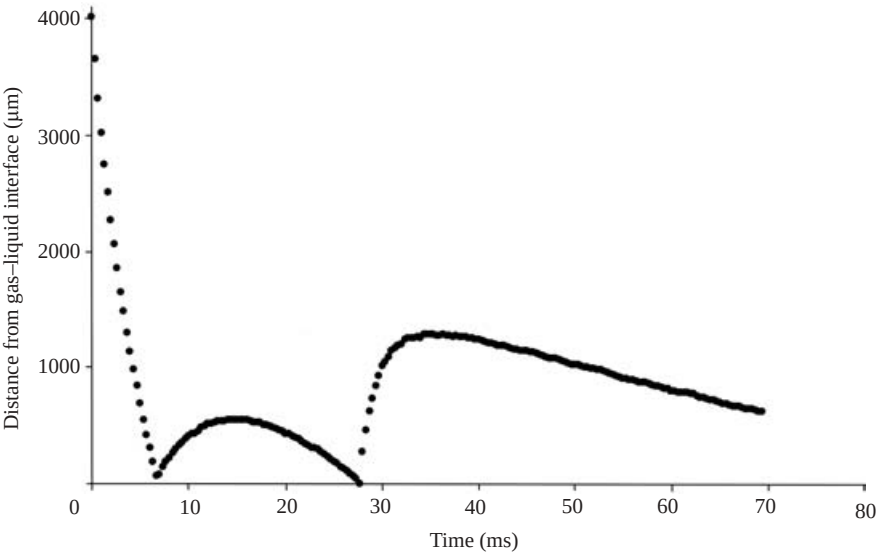

FIGURE 15. A sample trajectory showing a droplet bouncing once, then coalescing on the second impact. The coalescence is followed by the formation of a daughter drop with a larger velocity and smaller radius than the coalescing drop.

range. In some instances, we observed the formation of a granddaughter drop after the daughter drop coalesced. However, the very high velocity and small radius of this third generation of drop made observation difficult and so we report quantitative results only for the daughter drops.

The surprisingly high velocity of the daughter drop can be understood when we recognize that its formation is driven by surface tension forces. The Weber number of the coalescing drops was typically smaller than one, indicating that the inertia of the mother drop is small compared with the surface tension force generated when the gas film separating the drop and liquid sublayer ruptures. Thus, the daughter drop in our experiments with $We \leqslant O(1)$ is generated primarily by a surface-tension-driven flow. For collisions with $We \ll 1$, the surface-tension-driven velocity is larger than the impact velocity. This situation is similar to that studied by Thoroddsen & Takehara (2000) in which drops with diameters of about 3 mm were placed at an interface with essentially zero velocity so that $We = 0$. In contrast, the daughter drop formation observed for $We > 32$ by Rein (1996) and Hsiao, Lichter & Quintero (1998) results from a flow driven by the inertia of the impacting drop.

In general, we might expect the radius a_d and velocity U_d of the daughter drop to depend on the viscosities, μ_l and μ_g, and densities, ρ_l and ρ_g, of the liquid and gas, the surface tension σ, the velocity U and radius a of the mother drop, and the mean free path of the gas λ. However, the large ratio of the liquid to gas density suggests that the gas inertia is unimportant. The Ohnesorge numbers, Oh_l and Oh, based on the liquid and gas viscosity are small so that viscous stresses will play a small role in surface-tension-driven flows. If the viscosity of the gas is unimportant, then so is the mean free path. Thus, from dimensional analysis we conclude that a_d/a and $U_d(\rho_l a/\sigma)^{1/2}$ are functions of We only. These quantities will approach constant values when $We \ll 1$. In this limit, the impact velocity of the mother is small compared with the characteristic surface-tension-driven velocity scale $(\sigma/(\rho_l a))^{1/2}$ and the daughter formation is independent of the impact velocity.

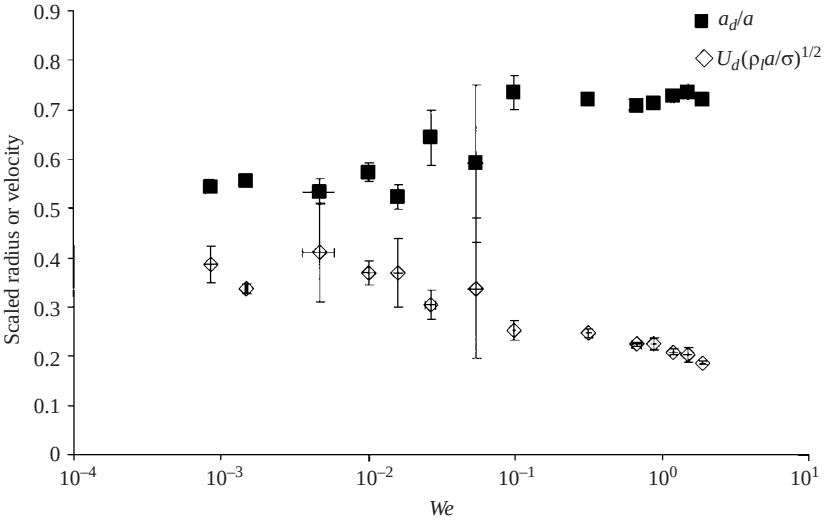

FIGURE 16. The ratio of the radius of the daughter and mother drop radii (diamonds) and the non-dimensional velocity $U_d(\rho_l a/\sigma)^{1/2}$ (squares) are plotted as a function of the Weber number based on the mother's radius and impact velocity. Each point represents an average over several observations with similar Weber numbers. The vertical error bars correspond to the 95% confidence intervals.

We found, as expected, that the daughter drop radius and velocity are independent of the gas composition and pressure and so we present the results for all pressures and both methane and nitrogen as the gas phase in figure 16. Because of the large velocity and small size of the daughter drop, considerable uncertainty was involved in the image analysis and trajectory fit that yielded the initial velocity of the daughter drop and the drop radius. To improve the statistical accuracy of the results, we averaged several observations of drop impacts with similar Weber numbers to obtain each point in figure 16. The ratio of the radii of the daughter and mother drops approaches $a_d/a = 0.55 \pm 0.02$ (95% confidence intervals) for $We \ll 1$. This is comparable to the value of about 0.54 that we estimate from figure 2 of Thoroddsen & Takehara. The dimensionless daughter velocity approaches $U_d(\rho_l a/\sigma)^{1/2} = 0.38 \pm 0.04$ for $We \ll 1$. Thoroddsen & Takehara did not report this quantity. However, they did visualize the detailed process of daughter formation (which is beyond the time resolution for our drop size and video system) and noted that the temporal duration of the drop-formation process follows a scaling obtained by balancing surface tension with inertia. This observation is consistent with the surface-tension–inertia scaling we observe for the daughter drop velocity. Note that, if the net surface energy released by the coalescence of the mother and formation of a smaller daughter drop were converted to the kinetic energy of the daughter with perfect efficiency, the dimensionless velocity would be $U_d(\rho_l a/\sigma)^{1/2} = 5.02$. Thus, not surprisingly, only a small portion of the energy goes into the translation of the daughter drop.

When the Weber number becomes $O(1)$, the radius ratio and dimensionless daughter velocity can have a dependence on *We*. We observed a slight increase in the ratio of the daughter to mother radius to a value around 0.7 and a decrease in the dimensionless velocity to about 0.2 for $We \approx 1$. A transition from coalescence with no daughter formation to the formation of daughter drops with increasing *We* has been observed at a much higher Weber number ($We = 32$) than those explored in our study (Rein 1996;

Hsiao *et al.* 1998). It is possible that the downward trend in daughter velocity with increasing Weber number for $We = O(1)$ is suggestive of the approach of a transition from daughter formation to no daughter formation at a Weber number intermediate between the highest value ($We = 2$) studied here and the much higher Weber numbers explored by Rein and Hsiao *et al.*

7. Conclusion

We have observed the transition from coalescence to bouncing with increasing Weber number for small (40 and 80 μm diameter) water drops colliding with a water sublayer in gases with various pressures and viscosities. The experimental results were compared with a theory based on potential flow in the liquid, weak deformation of the gas–liquid interfaces, and non-continuum viscous flow in the lubrication gas film. Both theory and experiment indicate a very strong dependence of the critical Weber number on the gas pressure and viscosity. Similar results were predicted for the coalescence–bounce transition in the head-on collision of two drops. This observation implies that, by varying the pressure in a heat exchanger or other multiphase flow, we may be able to observe an abrupt transition from a situation in which disperse droplets coalesce readily with a liquid film and with one another to one where the drops bounce and remain dispersed. We also observed and predicted the coefficient of restitution for drops that bounce. The coefficient of restitution is small owing to the highly deformable nature of the surface of the liquid sublayer and the generation of surface waves. Finally, we observe that a new smaller drop is formed at a gas–liquid interface after a drop coalesces. This smaller drop has a velocity that scales as a surface-tension-driven flow, i.e. $(\sigma/(\rho_l a))^{1/2}$. This phenomenon may play a role in the formation of fine mists and salt particles from the surface of the ocean.

The asymptotic theory presented here provides a good qualitative description of the coalescence–bounce transition and the coefficient of restitution and their dependence on the Knudsen, Weber and Ohnesorge numbers. The present theory is strictly valid only for very small Weber numbers. A computational method capable of describing large-amplitude deformation of the gas–liquid interfaces while also including an accurate description of the non-continuum gas flow acting in the thin gas film between the drop and interface would be needed to obtain a more robust theory capable of describing droplet coalescence and bouncing at moderate Weber numbers.

This work was supported by US Environmental Protection Agency grant R827115 and NASA grant NAG3-2349. The experiments concerning the formation of drops after coalescence were performed with the help of an undergraduate researcher, Manuel Balseiro, who was supported by the GE Faculty of the Future program.

REFERENCES

Brazier-Smith, P. R., Jennings, S. G. & Latham, J. 1972 The interaction of falling water drops: coalescence. *Proc. R. Soc. Lond.* A **326**, 393.

Cercignani, C. & Daneri, A. 1963 Flow of a rarefied gas between two parallel plates. *J. Appl. Phys.* **34**, 3509.

Clift, R., Grace, J. R. & Weber, M. E. 1978 *Bubbles, Drops and Particles*, p. 111. Academic.

Foote, G. B. 1975 The water drop rebound problem: dynamics of collision. *J. Atmos. Sci.* **32**, 390.

Gopinath, A. & Koch, D. L. 2001*a* Collision and rebound of small droplets in an incompressible continuum gas. *J. Fluid Mech.* **454**, 145.

Gopinath, A. & Koch, D. L. 2001*b* Dynamics of droplet rebound from a weakly deformable gas–liquid interface. *Phys. Fluids* **13**, 3526.

Hocking, L. M. 1973 The effect of slip on the motion of a sphere close to a wall and of two adjacent spheres. *J. Engng Maths* **7**, 207.

Hsiao, M., Lichter, S. & Quintero, L. 1998 The critical Weber number for vortex and jet formation for drops impinging on a liquid pool. *Phys. Fluids* **31**, 3560.

Jayaratne, O. W. & Mason, B. J. 1964 The coalescence and bouncing of water drops at an air/water interface. *Proc. R. Soc. Lond.* A **280**, 545.

Lee, M. M. & Hanratty, T. J. 1988 The inhibition of droplet deposition by the presence of a liquid wall film. *Intl J. Multiphase Flow* **14**, 129.

Nobari, M. R., Jan, Y.-J. & Tryggvason, G. 1996 Head-on collision of drops – a numerical investigation. *Phys. Fluids* **8**, 29.

Qian, J. & Law, C. K. 1997 Regimes of coalescence and separation in droplet collision. *J. Fluid Mech.* **331**, 59–80.

Rein, M. 1996 The transitional regime between coalescing and splashing drops. *J. Fluid Mech.* **306**, 145.

Rother, M. A., Zinchenko, A. Z. & Davis, R. H. 1997 Buoyancy-driven coalescence of slightly deformable drops. *J. Fluid Mech.* **346**, 117.

Schotland, R. M. 1960 Experimental results relating to the coalescence of water drops with water surfaces. *Disc. Faraday Soc.* **30**, 72.

Sundararajakumar, R. R. & Koch, D. L. 1996 Non-continuum lubrication flows between particles colliding in a gas. *J. Fluid Mech.* **313**, 283.

Thoroddsen, S. T., Etoh, T. G. & Takehara, K. 2003 Air entrapment under an impacting drop. *J. Fluid Mech.* **478**, 125.

Thoroddsen, S. T. & Takehara, K. 2000 The coalescence cascade of a drop. *Phys. Fluids* **12**, 1265.